海馬齒狀迴內具小白蛋白的中間神經元之突觸的同質性原則

A Synaptic Homogeneity Principle for Parvalbumin-Expressing Interneuron Synapses in the Hippocampal Dentate Gyrus

研究生：陳玠汝 (Chieh-Ju Chen)

指導教授：連正章 博士 (Cheng-Chang Lien, M.D., Ph.D.)

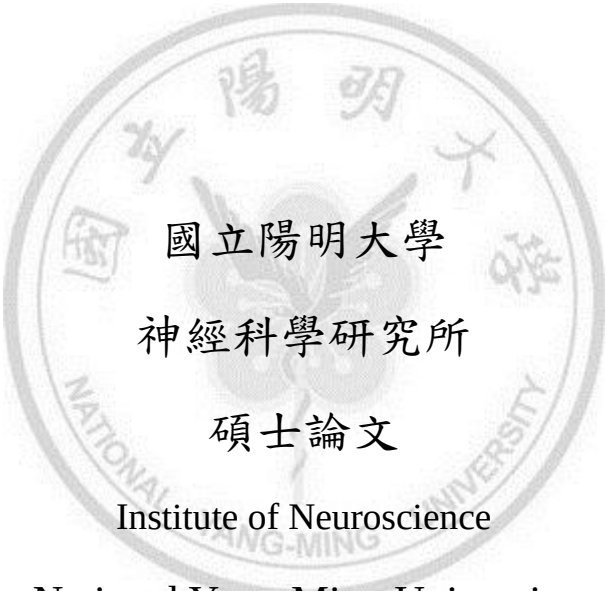

國立陽明大學

神經科學研究所

碩士論文

Institute of Neuroscience

National Yang-Ming University

Master Thesis

中華民國一〇四年二月

February, 2015

誌謝

兩年半的研究成果，這本論文將獻給那些被犧牲的生命。

首先感謝指導教授連老師，謝謝您提供優質的研究環境讓我學習先進的技術，並帶領我認識神經電生理的領域，並且謝謝您的教導以及花費不少時間來修正我的論文。感謝口試委員孫興祥、曹美玲、林惠菁老師在我的口試提供實驗的改良以及論文需要加強的部分，並讓我重新檢視這個研究的意義與價值。謝謝神研所老師們所提供紮實的課程，讓我收穫良多。

感謝實驗室的學長們，翁儒韻、劉于超、簡大鈞、江柏翰、李政達、侯文賢、陳建錞、許至緯在實驗上給我的幫助或是教導，尤其謝謝劉于超在我還是研究生的嬰兒時期帶領我使用電生理的儀器設備及實驗上觀念的建立，還有謝謝李政達和侯文賢幫助我對 paper 的理解。感謝黃嘉怡學姐的雞胚胎實驗及吳煜舜的 HEK 細胞讓我一開始有練兵的 side projects。感謝 Optogenetics 組的好夥伴們，許璨庭、顏廷耘、侯文賢可以在實驗上互相幫助及討論。感謝隔壁家實驗室及曾經的好鄰居張文瀚，謝謝你常常在我肚子餓的時候給我食物吃並且願意跟我換很多很多的一塊錢。感謝詹筑方、曹茵絪、陳亭伃在實驗室的陪伴與指導以及實驗室外的娛樂，感謝常常一起吃飯的歡樂夥伴們:詹筑方、李政達、侯文賢、江柏翰、高敏華、林昱伶、顏廷耘、謝瑀、陳勤霖，謝謝你們陪我一起吃飯聊天，其中感謝林昱伶和踢歪歪所帶來的歡樂!

還有我的同班同學們，顏廷耘、杜柏澔、張宇晟、李俐旻、張舒詠能一起分享研究上的心路歷程，另外我的好冰友們，小六、大美、滷咪和賀比，謝謝你們常常吸收我的喜怒哀樂。最後謝謝我的父母讓我可以無後顧之憂的專心在研究的領域上奮鬥。

陳玠汝　謹致於

國立陽明大學神經科學研究所

中華民國一百零四年二月

Chinese Abstract

海馬迴為學習和記憶功能相關的核區。在海馬迴中的齒狀迴結構是負責訊息進入的主要閘門。在齒狀迴的局部迴路中包含異質性的細胞族群，可根據不同的分子特性，細胞型態及電生理特質區分出γ-氨基丁酸型抑制型神經細胞。而其中，表現小白蛋白的神經細胞為細胞體抑制型神經細胞，它們對下游的神經細胞提供很強的抑制作用，此外它們在控制神經活性及調控神經的同步性中也扮演了很重要的角色。表現小白蛋白的神經細胞有高頻動作電位的特性，其軸突呈現樹枝狀散佈在齒狀迴的顆粒細胞層中，這些神經細胞可以支配顆粒細胞、非高頻動作電位細胞及高頻動作電位細胞。雖然從神經解剖學上的證據推測表現小白蛋白的神經細胞也會去支配在齒狀迴門區的細胞，包含門區的中間神經細胞(hilar interneuron)及苔蘚狀細胞(mossy cell)，但是表現小白蛋白的神經細胞和齒狀迴門區的神經細胞之間的功能性聯結仍不清楚。因此，我們結合光遺傳學搭配電生理學的技術去探討這個問題。我們的結果發現顆粒細胞和齒狀迴門區的中間神經細胞及苔蘚狀細胞相比，顆粒細胞從表現小白蛋白的神經細胞端接受了很強的突觸性訊號。然而，當不同時間性的抑制性訊號傳入顆粒細胞、齒狀迴門區的中間神經細胞及苔蘚狀細胞時並沒有任何顯著性的差異，這也暗示在表現小白蛋白的神經細胞跟它主要去支配的目標細胞的突觸，有著目標細胞非相關性的短期突觸增益效應。根據表現小白蛋白的神經細胞可以扮演著 γ 振盪產生器的角色並且調控顆粒細胞的同步作用，我們接著測試表現小白蛋白的神經細胞是否能調控門區細胞的同步作用。我們的結果呈現表現小白蛋白的神經細胞可能調控細胞的同步作用，並且是根據抑制性的聯結強度及門區突觸後細胞的特性。

English Abstract

The hippocampus is a key brain structure for learning and memory. The dentate gyrus (DG) serves as a primary gate of the hippocampus. Local-circuit GABAergic inhibitory interneurons (INs) in the DG comprise a heterogeneous cell population with distinct molecular, morphological, and electrophysiological properties. Among them, parvalbumin expressing (PV^+) INs are perisomatic INs that provide powerful inhibition to their downstream neurons. They also play an important role in controlling neuronal activity and therefore mediate neuronal synchronization. PV^+ INs show fast-spiking (FS) firing pattern and exhibit extensive axonal arborization within the DG granule cell (GC) layer. They innervate GCs, non-FS INs, and FS INs in the GC layer with high connection rates. Although anatomical evidence suggests that PV^+ INs also innervate hilar neurons (HNs), including hilar mossy cells (MCs) and hilar interneurons (HINs), the functional connections between PV^+ INs and HNs remain unknown. Here, we combined optogenetics with electrophysiology to address this question. Our results showed that GCs receive strong synaptic inputs from PV^+ INs compared to MCs and HINs. However, the temporal dynamics of inhibitory inputs to GCs, MCs, and HINs are not significantly different, indicating that synapses between PV^+ INs and their target cells display target cell-independent short-term synaptic plasticity. Given that PV^+ INs can function as a gamma oscillation generator and mediate synchronization of GCs, we next tested whether PV^+ INs mediate synchronization of HNs. Our results indicate that PV^+ INs can mediate synchronization of HNs, depending on the strength of inhibitory connections and postsynaptic HN identities.

Contents

Abbreviations

AAV: adeno-associated virus

AP: action potential

BC: basket cell

C/A: commissural/associational

ChR2: channelrhodopsin-2

DG: dentate gyrus

DPSS: diode-pumped solid-state

FS: fast-spiking

GC: granule cell

GCL: granule cell layer

HIN: hilar interneuron

HN: hilar neuron

IN: interneuron

ITI: inter-trial interval

IPSC: inhibitory postsynaptic current

MC: mossy cell

NpHR: halorhodopsin

PP: perforant path

PV: parvalbumin

Introduction

The hippocampus

The hippocampus is named after its anatomical shape which resembles seahorse, from the Greek "*hippo*" meaning horse and "*kampos*" meaning sea monster. The hippocampus is a key brain structure for learning and memory (O'Keefe and Dostrovsky, 1971; Leutgeb et al., 2007; Moser et al., 2008), especially for declarative memory and spatial navigation (Squire, 1992). The hippocampus comprises two parts, the dentate gyrus (DG) and CA regions (Cornu Amonnis, commonly divided into the CA1, CA2, and CA3 subregions). The subfields of the hippocampus have a well laminated organization and the tightly packed cell bodies form an interlocking C-shaped arrangement. The DG serves as the primary gate of the hippocampus. Cortical neurons carry major input and project their axons to the DG through perforant paths (PPs). They form synapses with glutamatergic excitatory principal cells, namely, granule cells (GCs) and local-circuit GABAergic inhibitory interneurons (INs) (Han et al., 1993; Freund and Buzsáki, 1996). Principal GCs send their axons called mossy fibers toward the CA3 area. The highly specialized mossy fibers form synapses on the proximal dendrites of CA3 principal cells and provide strong synaptic excitation onto CA3 principal cells (Geiger and Jonas, 2000; Rollenhagen et al., 2007). CA3 neurons in turn project to ipsilateral CA3, CA2 and CA1 neurons and contralateral CA3, CA2 and CA1 through the projections called Schaffer collaterals/associational pathways and commissural projections, respectively (Schaffer, 1892; Szirmai et al., 2012). The output station of the hippocampus is the CA1 area. Finally, CA1 neurons project output axons to layer V neurons in the entorhinal cortex and/or the neurons in the subiculum (Naber and Witter, 1998; Ishizuka, 2001). Thus the entorhinal-hippocampal circuit forms a

closed-loop processing that computes the cortical sensory information.

Dentate gyrus microcircuits

The DG serves as the primary gate of the hippocampus and thus controls information processing. Information transferred from the entorhinal cortex layer II to the DG through the PPs. The PPs innervate GCs and local INs. The axon collaterals of GCs innervate mossy cells (MCs) and INs in the hilus. Hilar interneurons (HINs) also send axons to innervate GCs (Acsády et al. 1998). Other GABAergic INs are also involved in information processing in the DG microcircuits. Parvalbumin-expressing (PV^+) basket cells (BCs) innervate GCs and provide short-term plasticity (Kraushaar and Jonas, 2000). Thus, feedforward inhibition arises when excitatory afferent inputs from cortical areas and activates both GCs and local GABAergic INs, which in turn inhibit GCs. Feed-back inhibition arises when a small population of GCs activate GABAergic INs which exert fast and strong inhibition on the non-coding GCs, respectively (Liu et al., 2014). The MCs form hilar commissural/associational (C/A) projections to innervate the GCs of the ipsi- and contralateral DG (Nakashiba et al., 2008).

GABAergic INs in the DG

Local-circuit GABAergic inhibitory INs in the DG comprise a heterogeneous cell population with distinct molecular, morphological, and electrophysiological properties (Freund and Buzsáki, 1996; Somogyi and Klausberger, 2005; Hosp et al., 2014; Liu et al., 2014). They are divided into two classes, soma-targeting and dendrite-targeting INs (Freund and Buzsáki, 1996). These two classes of inhibitory INs mediate the inhibitory control and also provide distinct spatiotemporal control over GC activity (Pouille and Scanziani, 2001). In the DG, a class of soma-targeting INs, PV^+ BCs, generate reliable

and powerful phasic inhibition onto GCs (Kraushaar and Jonas, 2000). PV^+ INs are a type of inhibitory INs and play an important role in controlling neuronal activity and therefore mediate neuronal synchronization (Cobb et al., 1995; Bartos et al., 2007). In contrast to soma-targeting INs, dendrite-targeting INs are more complex and heterogeneous. According to previous studies (Han et al., 1993; Freund and Buzsáki, 1996; Hosp et al., 2014; Liu et al., 2014), dendrite-targeting neurons include hilar perforant path-associated cells (HIPPs), hilar C/A path-associated cells (HICAPs), and total molecular layer interneurons (TMLs). Dendrite-targeting INs are involved in regulating dendritic electrical and biochemical signaling and synaptic plasticity (Miles et al., 1996; Leão et al., 2012; Chiu et al., 2013；Hosp et al., 2014).

Mossy cells in the hilus

There are two classes of glutamatergic principal cells in the DG. One is GCs, which are the vast majority cells in the DG, and the other is MCs, which are the least numerous cell type in the hilar region (Amaral et al., 1990; Henze and Buzsáki, 2007; Scharfman and Myers, 2013). MCs have characteristic appearance called thorny excrescences because the appearance of proximal dendrites with numerous large spines (Amaral, 1978). The soma and dendrites of MCs are restricted in the hilus. The hilar MCs form the C/A afferents in the both dentate gyri and innervate proximal dendrites of GCs within the inner molecular layer. MCs are known to be highly excitable. They receive large, frequent barrages of spontaneous synaptic input (Ishizuka and Kosaka, 1998) from a small number of GCs and provide a strong excitatory output to a large numbers of GCs. The excitatory commissural afferents that originate from the MCs have a net inhibitory effect on GCs via activation of inhibitory neurons (Buzsáki and Eidelberg, 1981; Douglas et al., 1983; Santhakumar et al. 2000; Jinde et al., 2012). Due to the

unique connections, MCs have been suggested to play an important role in normal signal processing in learning and memory, especially pattern separation (Lisman, 1999; Myers and Scharfman, 2009; Jinde et al., 2012).

Specific Aims

In the hippocampus, PV^+ BC INs are mostly fast-spiking (FS) and innervate to the perisomatic area of target cells. They can target to GCs and function as a gamma oscillation generator (Cobb et al., 1995; Bartos et al., 2007). Although there is apparent anatomical evidence that PV^+ INs innervate hilar neurons (HNs) (Acsády L et al. 2000; Murakawa and Kosaka, 2001), little is known about the functional connections between PV^+ INs and HNs and the network function. In this study, I combined optogenetics with electrophysiological recordings to address two fundamental questions. First, I recorded the postsynaptic target cells to examine the functional connection. Second, I performed simultaneous dual recording from two HNs by using cell-attached recording and study whether PV^+ INs mediate synchronization of HNs.

Materials and Methods

Animals

PV-cre (B6;129P2-*Pvalb*$^{tm1(cre)Arbr}$/J) knock-in mice (aged 4-8 weeks) were obtained from The Jackson Laboratory (008069; Bar Harbor, ME, USA). Mice were maintained on a reverse 12 hr light/dark cycle and were given food and water *ad libitum*. All experimental procedures involving animals were performed and approved by the Institutional Animal Care and Use Committee of National Yang-Ming University.

Acute hippocampal slice preparation

PV-cre mice were anaesthetized with isoflurane and killed by rapid decapitation, in accordance with national and institutional guidelines. Mice brains were rapidly removed and 300 μm thick coronal hippocampal slices were cut in ice-cold sucrose solution containing the following (in mM): 87 NaCl, 25 $NaHCO_3$, 1.25 NaH_2PO4, 2.5 KCl, 10 glucose, 75 sucrose, 0.5 $CaCl_2$, and 7 $MgCl_2$ using a vibratome (DTK-1000, Dosaka). Slices were incubated in oxygenated (95% O_2, 5% CO_2) sucrose solution in a holding chamber at 34 ℃ for 30 min and stored in the chamber at room temperature until used.

Virus preparation

We obtained the channelrhodopin-2 (ChR2)-expressing viruses from two resources: First, an adeno-associated virus serotype 5 (AAV5) vector (AAV5-EF1α-DIO-hChR2(H134R)-eYFP-WPRE-hGH or AAV5-EF1α-DIO-hChR2(H134R)-mCherry-WPRE-hGH) was produced by University of North Carolina Vector Core Facilities (Chapel Hill, NC, USA). Second, an AAV5 was generated and purified by our

collaborator Dr. Tai, Min-Hong's laboratory in the National Sun Yat-Sen University (Kaohsiung, Taiwan). The ChR2-eYFP transgene construct, the packaging (pLT-RC03) and adeno helper constructs (pHGTI-Adeno1) were needed for the virus generation. The transgene, packaging and helper constructs were transfected into E1α-transformed human embryonic kidney 293 (HEK293) cells by calcium phosphate method. All transgene constructs are gifts from Dr. Karl Deisseroth (Standford University, CA). The viral packaging and helper constructs are gifts from Dr. Lee, Jeng-Shin (Harvard Gene Therapy Initiative, Harvard Medical School, Boston, MA, USA). To silence the PV^+ INs in the behavior experiment, an AAV5 carrying cre-inducible halorhodopsin (NpHR)-eYFP transgene (AAV-EF1α-DIO-eNpHR3.0-eYFP) would be expressed on the PV^+ INs, whereas an AAV5 carrying cre-inducible eYFP transgene (AAV-EF1α-DIO-eYFP) was used for the control experiment. These two viruses were produced by University of North Carolina Vector Core Facilities (Chapel Hill, NC, USA).

Stereotaxic microinjection and optical fiber implantation

Mice (aged 4-8 weeks) were housed in the animal center with food and ad libitum water until surgery. Mice were anaesthetized with 4 % isoflurane (vol/vol; Halocarbon Laboratories, North Augusta, SC, USA) mixed with 100 % oxygen in the chamber, and their heads were shaved for further operation. Mice were placed on a homeothermic blanket to keep the body temperature constant (34 °C) and mounted in a stereotaxic apparatus (Stoelting Co., Wood Dale, IL, USA) and kept under constant isoflurane air flow (2.25 mL/hour) anesthesia during surgery. High titers of AAV type 5 or 8 carrying ChR2 tagged with eYFP or mCherry were microinjected into the dorsal hippocampal DG (coordinates from Bregma: Anterior-Posterior: -2 mm; Medial-Lateral: 1.7 mm; Dorsal-Ventral: -2 mm and -1.8 mm), using a 10 μl NanoFil syringe (World Precision

Instruments, Sarasota, Florida, USA) and a 35-gauge beveled metal needle. Injection volume (0.5 μl at each site) and the flow rate (0.1 μl/min) will be controlled with a nanopump Controller (KD Scientific, Holliston, MA, USA). The 35-gauge steel was held in place 0.1 mm above the injection site for 10 min after injection before being slowly withdrawn. For the behevior experiment, an AAV carrying eNpHR3.0 tagged with eYFP or mCherry was bilaterally microinjected into the DG (Anterior-Posterior: -2 mm; Media-Lateral: ± 1.7 mm; Dorsal-Ventral: -2 mm and -1.8 mm). The fiber-optic cannula for implantation consisted of a ferrule (1.25 mm in diameter and 6.4 mm long; Precision fiber product, Inc) and flat tip of an optical fiber (230 μm in diameter). The implantation of fiber-optic cannula into the DG for illumination of PV^+ IN was performed immediately after injection of viruses. To fix the fiber-optic cannula on the skull, C&B Superbond (Sun Medical) was applied to the surface of the skull around the cannula for 10 min. After the C&B Superbond hardened, the cannula was released from the home-made holder. Dental cement (GC corporation, Tokyo, Japan) was applied around the cannulation site. After virus injection and optical fiber implantation, mice were returned to their home cage for at least 3 weeks to allow for virus expression.

Electrophysiology and optical stimulation

During experiments, individual slices were placed in a recording chamber and continuously perfused with oxygenated artificial cerebrospinal fluid (ACSF) containing the following (in mM): 125 NaCl, 25 $NaHCO_3$, 1.25 NaH_2PO_4, 2.5 KCl, 25 glucose, 2 $CaCl_2$, and 1 $MgCl_2$. The recording temperature was at room temperature (23 ± 2 ℃). The ChR2-eYFP or ChR2-mCherry expression pattern was confirmed with fluorescence light (510 nm or 530 nm wavelength) by Xenon lamp and images were taken by EM-CCD camera (QuantEM 512SC, Photometrics, USA). ChR2 was excited

by blue light (470 nm; LED4D162, controlled by DC4104 driver, Thorlabs), which was delivered directly through the objective, the optical stimuli were simultaneously recorded by a GaP photodiode (wavelength range: 150-550 nm, 1ns rise time, Thorlabs). Whole-cell recordings were made using a Multiclamp 700B amplifier (Molecular Devices, Sunnyvale, CA, USA). Recording electrodes (3–6 MΩ) were pulled from borosilicate glasses with filament (outer diameter, 1.5 mm; inner diameter, 0.86 mm; Harvard Apparatus, Holliston, MA, USA). For performing patch-clamp recordings on postsynaptic neurons, recording pipettes were filled with high Cl^- internal solution containing the following (in mM): 15 K-gluconate, 140 KCl, 0.1 EGTA, 2 $MgCl_2$, 4 Na_2ATP, 10 HEPES, and 0.4 % biocytin (g/ml; Life Technologies, Grand Island, NY, USA) (osmolarity: 310 mOsm/L). For recordings on ChR2-eYFP-expressing neurons, recording pipettes were filled with internal solution containing the following (in mM): 120 K-gluconate, 24 KCl, 0.2 EGTA, 4 MgATP, 10 HEPES, 7 Na_2-phosphocreatine, 0.5 NaGTP, and 0.4 % biocytin (4 mg/ml). For the investigation of the inhibitory effect of PV^+ INs and their target cells, recording pipettes were filled with low Cl^- internal solution containing the following (in mM): 136.8 K-gluconate, 7.2 KCl, 0.2 EGTA, 4 MgATP, 10 HEPES, 7 Na_2-phosphocreatine, 0.5 Na_3GTP (pH 7.3 with KOH) and 0.5 % biocytin. The light-evoked IPSPs were recorded in the current-clamp configuration. For the detection of spontaneous spike responses of HNs, cell-attached recordings (pipette resistance 4–7 MΩ) were performed (Lien et al., 2006). To increase the spiking activities, 10 μM carbarchol were applied in the cell-attached and current-clamp recordings. For all recordings, pipette capacitance was almost fully compensated. Series resistance (R_s) was compensated to ~80% in the voltage-clamp configuration. Signals were low-pass filtered at 4 kHz and sampled at 10 kHz using Digidata 1440A (Molecular Devices). A Digidata 1440 A connected to a personal computer was used for stimulus generation and data acquisition. Pulse sequences were generated by

pClamp 10.4 (Molecular Devices). All recordings were made at 22–24˚C.

Biocytin filling and *post-hoc* morphological recovery

To identify the morphology of target cells, neurons were loaded with biocytin (4 mg/ml, dissolved in intracellular solution) during whole-cell recording for at least 30 min. Subsequently, sections were fixed overnight in 4 % paraformaldehyde, washed and stored in 0.1 M PBS. After washing with 0.1 M PBS, slices were incubated with Alexa 594 or Alexa 488 conjugated avidin (1:400; Invitrogen, Carlsbad, CA, USA) in 0.1 M PBS and 0.3 % triton X-100 overnight at 4 ˚C. After wash three times for 20 minutes, slices were embedded in Vectashield mounting medium (Vector Laboratories, Burlingame, CA, USA). We used two-photon microscope to examine the labelled cells with a pulsed titanium: sapphire laser (Chameleon-Ultra II tuned to 800 nm for Alexa-594 and 720 nm for Alexa 350; Coherent, Portland, OR, USA) attached to a Leica DM6000 CFS (Leica, Wetzlar, Germany) that was equipped with a 20x/1.0 numerical aperture (NA) water immersion objective (HCX APO L; Leica, Wetzlar, Germany). For identification of ChR2-eYFP-labelled PV^+ cell, we used EM-CCD camera (QuantEM 512SC, Photometrics, USA) coupled with MetaFluor software (Molecular Devices, USA). The ChR2-eYFP expression pattern was imaged by confocal microscopy (Leica DM6000 CFS).

Contextual fear conditioning and *in vivo* photo-stimulation

For animal behavior experiments, mice were handled at least 2 days before performing the behavior test (Hurst and West 2010). Contextual fear conditioning was performed in the chamber two days. The chamber (17.8 × 17.8 × 30.5 cm, Coulbourn Instruments) was equipped with shock floor which consisted of stainless-steel rods was used to

deliver the foot shock. On Day 1, optical fibers were attached through optical fiber cable which contained an FC/PC adaptor (Precision fiber product, Inc) and coupled to a 589 nm, diode-pumped, solid-state (DPSS) laser (OEM Laser Systems, Midvale, UT, USA). Next, mice were placed into the chamber to habituate for 2 min. After 2-min habituation, mice received 3 trials (ITI, inter-trial interval: 1 min) of foot shock (0.6 mA, 2 s) in the following 3 min. The yellow light was delivered through the optical fiber from the 589 nm DPSS laser during the training period. The chamber was cleaned with 70 % ethanol before and after each session. After the last shock, mice were observed for 1 min and then returned to the home cage. Twenty-four hours later, mice were first placed into the chamber for 5 min without foot shock and light to access the contextual fear, then followed by the light on for 5 min and light off for 5 min. After removal of optic fiber cable, mice returned to the home cage. To evaluate the fear learning in Day 1 training session, we recorded the freezing time in habituation and each trial, and recorded the freezing time during the total observation time in Day 2 contextual. The percentage of freezing time is calculated by following equation:

$$Freeezing\ (\%) = (total\ freezing\ time\ (s) / total\ observation\ time\ (s)) \times 100\ \%$$

The freezing time was defined as more than 2 s immobility, with crouching posture, except for respiratory response. Freezing behavior was scored post hoc by using the instantaneous time sampling.

Data analysis and statistics

The criteria for defining a responsive cell was based on the averaged IPSCs (at least 20 IPSCs). The cell was counted as a responsive cell only when its averaged peak IPSC amplitude is greater than 3-fold standard deviation (SD) of the baseline. Data were analyzed using Clampfit 10.4 (Molecular Devices) and Prism 5.0 (GraphPad Software,

San Diego, CA, USA). The decay of the uIPSC was fitted with a bi- exponential function. Data were presented as mean ± standard error of mean (SEM). Error bars represent SEM. Statistical significance was tested by the Wilcoxon-signed rank test and Kruskal-Wallis test. The significance level (p value) as indicated using Prism 5.0. To test if two HNs were synchronous firing, cross-correlation functions (Perkel et al., 1967; Nevet et al., 2007) were performed. Within a pair of two HNs, 10 spike trains were recorded simultaneously. One HN was taken as the reference cell, the other was target cell, and each reference spike were centered by the reference spiking time. We marked timing for each spike in the window and calculated a count of the spikes of the target cell at specific time delays with a 50-ms bin size for a time window of ± 500 ms. Finally, all count of spikes were summed in a time window, generating an accumulated histogram.

Results

Identification of PV^+ INs in the dorsal DG

By combining optogenetics and electrophysiology, I investigated the functional connections between PV^+ INs and MCs. The type 5 AAV carrying double-floxed ChR2-eYFP transgene under the control of EF1α promoter was injected into the unilateral side of dorsal hippocampal DG of PV-cre mice (Fig. 1A). The eYFP-labelled axons were mainly observed in the granule cell layer (GCL) and partially in the molecular layer and hilus at the virus injection side (Fig. 1B). To further confirm $eYFP^+$ cells expressing ChR2 (Fig. $2A_1$), I recorded $eYFP^+$ cells under IR-DIC configuration (Fig. $2A_2$). The recorded $eYFP^+$ cell displayed high-frequency (> 160 Hz at 23 ± 2 ℃) action potentials (AP) in response to depolarizing current pulses. The input resistance (R_{in}) of $eYFP^+$ cell was measured by injecting a hyperpolarizing (1 s; 100 pA) current step (R_{in}= 80 ± 10 MΩ) (Fig. 2B). Overall, the morphological and physiological properties are consistent with the description of PV^+ INs. I next determined whether the delivery of blue light can activate ChR2. APs and photo-currents were generated reliably by delivering 1 ms pulses of blue light (470 nm) (Fig. 2C). After *post-hoc* biocytin staining, I used Neuromantic software to reconstruct the morphology of the PV^+ IN (Fig. 2D).

Optical control of PV^+ INs

Next, I investigated the functional connections between the PV^+ INs and their postsynaptic neurons (Fig. 3). With 1 ms pulses of blue light, I recorded inhibitory postsynaptic currents (IPSCs) in single MCs and HINs in the presence of the ionotropic glutamate receptor antagonist kynurenic acid (2 mM) (Fig. $3B_1$, $3E_1$). The IPSCs were blocked after addition of the $GABA_A$ receptor antagonist SR 95531 (1 μM) (Fig. $3B_3$,

$3E_3$), indicating $GABA_A$ receptor-mediated transmission. Its short-term plasticity also showed multiple pulse depression (Fig. $3B_2$, $3F_2$). The recorded neurons were filled with biocytin and *post-hoc* recovered. The recorded cell was identified as MC by the soma and dendrites restricted in the hilus (Fig. 3C) and the distinctive morphology including the complex spines, so called thorny excrescences (Fig. 3C, box). The light-induced $IPSC_1$ was plotted against the light intensity (from 0 to 100 %). The $IPSC_1$ recorded in several neurons (n = 3) showed that 50 % light intensity (that is, LED power equals to 7.5 mW) was sufficient to induce maximum postsynaptic responses (Fig 4A). I next compared the synaptic properties of PV^+ IN-GC, PV^+ IN-MC, PV^+ IN-HIN synapses (Fig. 4). Dentate PV^+ IN-GC synapses showed stronger synaptic strength compared to PV^+ IN-MC and PV^+ IN-HIN synapses (Fig. 4B-F). The temporal dynamics of inhibitory inputs to GCs, MCs, and HINs was not significantly different (Fig. 4G-I), indicating that synapses between PV^+ INs and their target cells display target cell-independent short-term synaptic plasticity. To further investigate the inhibitory effect of PV^+ INs on target cell output, I first recorded light-evoked IPSPs in GCs and MCs in the current-clamp mode (held at -40 mV) in the presence of 10 μM carbarchol (Fig. $5A_1$, B_1). A single GC was held at -40 mV in current-clamp mode showed larger hyperpolarized potentials than MC in response to repetitive 5 Hz photo-stimulation (Fig. $5A_2$, B_2). The spike histogram of a single GC (Fig. $5A_3$) showed the less spike during photo-stimulation compared with that of a single MC (Fig. B_3). The data showed that PV^+ INs provide stronger inhibition on GCs than MCs.

PV^+ IN-mediated GABA release mediates synchronization between two HNs

Next, I investigated the PV^+-mediated network function. PV^+ INs provide precise

control of timing and probability of spike generation in target cells (Pouille and Scanziani, 2001). This characteristic could serve as a gamma oscillation generator and contribute to the synchronization of principal cells and the generation of fast network oscillations (Cobb et al., 1995; Buzsáki and Draguhn, 2004; Klausberger and Somogyi, 2008). To investigate the effect of PV^+ INs on oscillatory activity of target cells, I performed simultaneous cell-attached recording from two randomly selected HNs (including MCs and HINs). The spontaneous action currents were recorded from two HNs before and after photo-stimulation (Fig. $6A_1$, $6B_1$). We next tested the functional connections between PV^+ INs and HN1 and HN2. As illustrated (Fig. $6A_2$, $6B_2$), whole-cell recording from these two HNs showed that light-evoked IPSCs (Fig. $6B_1$, $6B_2$). To test if two HNs were synchronous firing, I performed cross-correlation analysis (Perkel et al., 1967; Nevet et al., 2007). During photo-stimulation, two HNs show tendency to synchronize together (Fig. $6A_3$). On the other hand, two HNs did not show the synchronization under 5 Hz stimulation (Fig. $6B_3$). The results indicated that PV^+ INs mediate synchronization of HNs, likely depending on inhibitory connections and postsynaptic HN identities.

Optical silencing of PV^+ INs in the DG

Given that DG is essential for generating contextual memories (Hernández-Rabaza et al., 2008). To investigate the function of PV^+ INs in the DG in the behavioral aspect, I performed *in vivo* optogenetics to bilaterally silence PV^+ axonal terminals in the DG. PV-cre mice were injected with either an AAV carrying halorhodopsin tagged with eYFP (AAV-DIO-eNpHR-eYFP) as the test group (NpHR group) or an AAV-DIO-eYFP as the control group. Mice were implanted with optical fibers after virus injection (Fig. 7B left). After one month, I performed the contextual fear learning test. On Day1,

optical fibers were attached through an FC/PC adaptor to the 589 nm DPSS laser. Next, mice were placed into the chamber box to habituate for 2 min. The yellow light (589 nm) was delivered through the optical fiber from the yellow laser during the training period. After 24 hours, mice were placed into the same chamber box to test the fear level (Fig. 7A right). I calculated the percentage of freezing time during the habituation, ITI_1, ITI_2, ITI_3 periods of training (Fig. 7B). All mice showed no freezing level during the habituation time. The result showed that the control group and NpHR group both increased the freezing time with the increasing times of foot shock (Fig. 7B). The data also indicated that mice with silencing PV^+ INs showed enhanced freezing levels during training. Next, I compared freezing levels of these two groups during the test period on Day 2. The freezing level up to 50 % showed that both groups can recall the fear memory (Fig. 7C), but the freezing levels showed no difference between these two groups (Fig. 7C). The result indicated that contextual fear learning did not affect memory retrieval on Day 2. These two groups also showed no difference in freezing level during the light-on period on Day 2, indicating the yellow light *per se* was not an associated cue during the contextual training. To further confirm that $eYFP^+$ cells expressed NpHR (Fig. $7D_1$), $eYFP^+$ cells were recorded in the whole-cell configuration (Fig. $7D_2$). As illustrated (Fig. $7D_3$), the APs of $eYFP^+$ cells were effectively suppressed during yellow light illumination. Taken together, PV^+ INs may play a role in pattern separation during learning.

Discussion

Summary

Overall, my results reveal the functional connections between PV^+ INs and their targets GCs, MCs and HINs. First, dentate PV^+ INs show stronger synaptic input to GCs than MCs and HINs. Second, the short-term plasticity between PV^+ INs and postsynaptic target cells are not significantly different, indicating target cell-independent short-term plasticity. Given that PV^+ INs can target GCs and function as a gamma oscillation generator, our results indicated that PV^+ INs may mediate synchronization of HNs, depending on the strength of inhibitory connections and postsynaptic HN identities.

The indirect influences of PV^+ INs on MCs or HINs

My work mainly focused on the direct innervations of PV^+ INs to MCs or HINs in the DG microcircuit. The results show that PV^+ INs send inhibitory output to MCs and HINs in the presence of ionotropic glutamate receptor antagonist (Fig. $3B_1$, $3E_1$). Given that GCs send their axons to innervate MCs and HINs, there may be a possibility that PV^+ INs can affect the activity of MCs or HINs through GCs. In this case, PV^+ INs may provide strong inhibition to GCs and decrease their activity. Therefore, the MCs and HINs activity were decreased. Taken together, PV^+ INs can decrease the activities of MCs and HINs through either direct innervations to MCs and HINs or indirect influences on GCs.

Over-bouton stimulation

Because the axon arbors of PV^+ INs were mainly restricted in the GCL, less axon collaterals were located in the hilus region. It is thus technically challenging to test the

functional connections between PV^+ INs and neurons located in the hilus by using paired recordings. To overcome this problem, we combined optogenetics and electrophysiology to address the functional connections between PV^+ INs and MCs and HINs. With fullfield, over-bouton illumination, we selectively activated genetically defined ChR2-expressing PV^+ INs and recorded their outputs in their target cells.

However, recent studies have shown that optically (over-bouton illumination) evoked synaptic currents often exhibited the artificial synaptic depression with the use of AAV2-ChR2 (Zhang and Oertner, 2007; Cruikshank et al., 2010; Olsen et al., 2012; Jackman et al., 2014). In our study, the IPSCs recorded in the target cells of PV^+ INs all show multiple-pulse synaptic depression. To exclude the possibility of artificial synaptic depression caused by AAV5-ChR2, we performed BC-GC paired recordings. Recordings from BC-GC pairs show that the degree of multiple pulse depression is similar to optically evoked synaptic responses. Therefore, it is likely that the synaptic depression of PV^+ IN-MC and PV^+ IN-HIN synapses are not caused by ChR2. We are aware that the decay time constant (12.41 ± 2.45, n = 6; Fig. 8A) recorded in BC-GC pairs was significantly shorter than that (21.88 ± 1.7, n = 12; $^{**}p < 0.05$, Wilcoxon-signed rank test) evoked by optical stimulation. The possible explanation is that optical stimulation evoked firing of multiple BCs with small jitters or caused by multiple spike generation in single BCs (see Fig. 8B-D).

The role of PV^+ IN-HN synapses

The sparse firing activity of GCs is thought to be important for pattern separation and spatial information encoding (Leutgeb et al., 2007; McHugh et al., 2007; Moser et al., 2008). GABAergic inhibition is known to contribute to the sparse firing of GCs. Previous studies suggest that GABAergic inhibition may directly target MCs, leading

to suppression of their excitatory effect on GCs (Scharfman, 1995). The inhibitory inputs to MCs are from terminals that contain PV or cholecystokinin and HIN (Acsády et al., 2000; Larimer and Strowbridge, 2008). Therefore, the innervation of MCs by PV^+ INs might play a role in pattern separation. My study is the first to provide functional evidence for PV^+ IN-mediated inhibition onto HNs. In the DG microcircuit, GCs are activated by the inputs from the entorhinal cortex. However, feed-forward and recurrent (feedback) inhibition and C/A inhibition provided by MCs limit the subsequent activation of the recently-activated GCs (Lisman, 1999; Jinde et al., 2012). Inhibition of MCs could also reduce the activation of these recently-activated GCs and may be important for functions related to pattern separation. Our data indicated that PV^+ INs can mediate synchronization of HNs at theta rhythm (see Fig. $6A_3$). MCs is capable of synchronizing a large number of GCs in the septotemporal axis of the hippocampus (Scharfman, 1995). Thus, we speculate that PV^+ INs may regulate the activity of GCs in the distal region through long-range projecting MCs. Intriguingly, the influence of PV^+ INs on the excitability of HNs in some cases is minimal, suggesting that the effect provided by PV^+ INs likely depend on the strength of inhibitory connections and postsynaptic HN identities. Because the type of ChR2 we used could not follow the high frequency photo-stimulation. We chose theta frequency to investigate the functional effect of PV^+ INs on HNs. In addition to theta oscillations, GABAergic INs, especially, PV-expressing subtypes, play a key role in the generation of gamma (30 – 80 Hz) oscillations in various regions of the brain (Bartos et al., 2007; Buzsáki and Wang, 2012; Varga et al., 2012). To examine whether PV^+ INs are involved in gamma oscillations in the hilar network, expression of ChR2 variant (pAAV-Ef1α-DIO-hChR2 (E123T/T159C)-mCherry) with fast kinetic in PV^+ INs is required for the future experiments.

PV^+ INs in the DG are involved in learning

Given that DG is essential for generating contextual memories (Hernández-Rabaza et al., 2008). At the behavioral level, suppression of PV^+ INs (i.e., disinhibition of pyramidal neurons) is necessary for certain forms of learning, whereas activation of PV^+ cells may promote extinction (Letzkus et al., 2011; Wolff et al., 2014; Sparta et al., 2014). At the network level, how inhibition driven by PV^+ INs regulates activities of local and remote GCs need to be examined. To understand the functional roles of PV^+ INs in the DG in the behavioral aspect, I will perform further behavioral tests related to learning and memory using *in vivo* optogenetic silencing technique. The behavioral tests that I plan to perform are the contextual fear test and novel object recognition test.

The preliminary data of contextual fear test suggest that NpHR group mice showed better learning behavior during training. In the contextual fear training test, a sustained and prolonged yellow light (589 nm) was delivered to inactivate PV^+ INs in the DG. The net effect of inhibiting PV^+ INs in the DG microcircuit might separate into two phases: the rapid excitation phase and following inhibition phase. At the mono-synaptic transmission level, silencing of PV^+ INs would cause disinhibition of GCs, thus enhancing the DG output. At the disynaptic transmission network level, the following inhibitory phase occurs as the disinhibition of other GABAergic INs would provide inhibition to GCs. On the other hand, the disinhibition of GCs may provide feed-back inhibition to inhibit other non-coding GCs. Recent studies indicated that distinct populations of neurons respond to a specific memory engram (Josselyn SA, 2010; Liu, et al., 2012). One possible explanation for our finding is that at the first foot shock under training, a sparse population of GCs are responsible for encoding the fear learning, and the inhibition of PV^+ INs under the second time of foot shock are more likely to activate

the same distinct population of GCs.

Future directions

The c-Fos staining is required to confirm the enhanced excitability of the GC population following optogenetic silencing of PV^+ INs. The location of implanted optical fibers need to be further checked. A fundamental question remains to be discussed. Previous studies showed that PV-expressing GABAergic neurons at the GCL/hilar border project contralaterally (Goodman and Sloviter, 1992). To solve these paradoxical findings, I plan to inject higher titers of AAV-ChR2 into the PV-cre mice and perform the immunostaining of eYFP, which can enhance the eYPF signal.

Figures

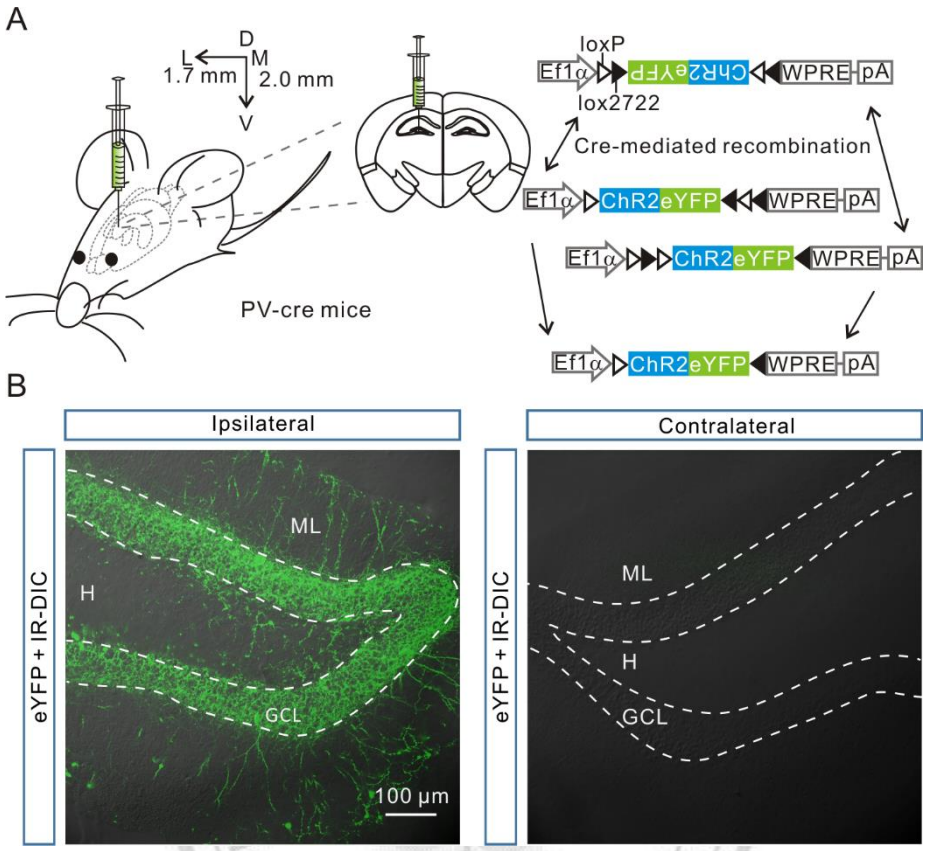

Figure 1. ChR2-eYFP expression in the DG

A. Scheme of injection of AAV5 carrying double-floxed inverted open reading frame (DIO) encoding ChR2-eYFP into the dorsal hippocampus of PV-cre mice. The Ef1α promoter driven transgene ChR2-eYFP shown on the right side. The PV^+ INs of the injection site can express ChR2-eYFP through Cre-Lox recombination. Axis: L, lateral; V, ventral; M, medial; D, dorsal.

B. Left: PV^+ INs and their axonal arborizations on the ipsilateral side of AAV injection. Right: the merge image of eYFP signal and IR-DIC image. Note that no eYFP expression was detected in the contralateral side. The borders of GCL are outlined. ML, molecular layer; H, hilus; GCL, granule cell layer.

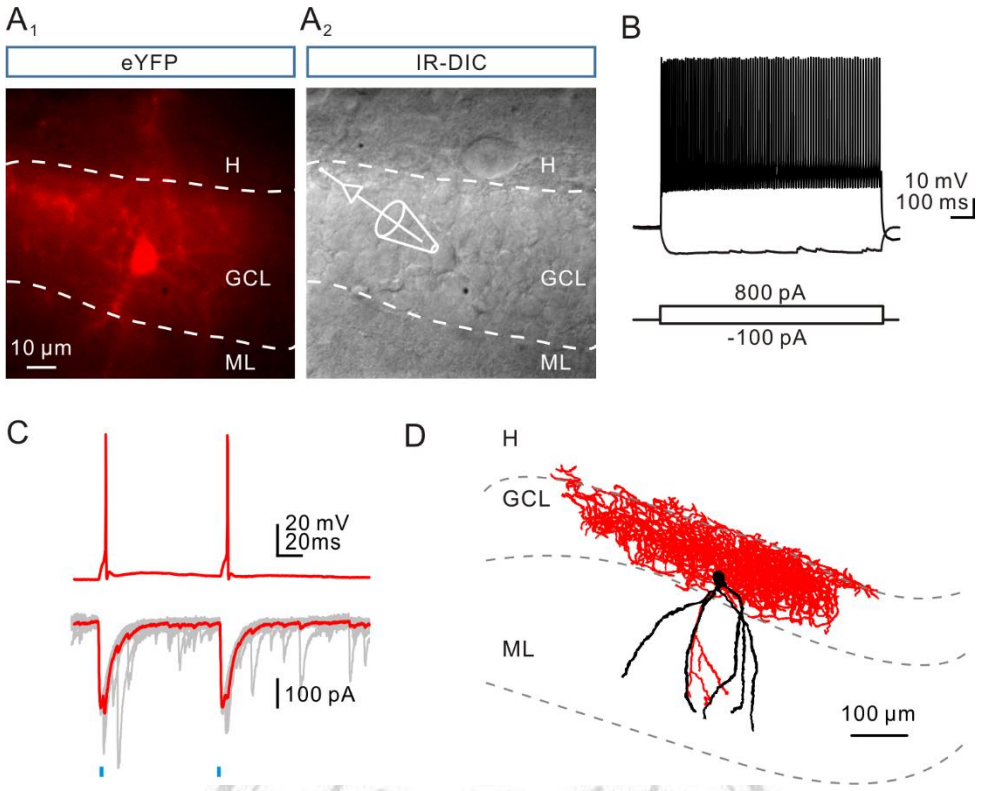

Figure 2. Light-evoked spikes and currents in fast-spiking INs

A_1. Fluorescence image of a ChR2-eYFP$^+$ neuron, suggesting PV$^+$ IN. The borders of GCL are outlined. H, hilus; GCL, granule cell layer; ML, molecular layer.

A_2. IR-DIC image of the recorded PV$^+$ IN shown in A_1.

B. High-frequency APs and hyperpolarized membrane responses elicited in the same ChR2-eYFP$^+$ neuron. The protocol was shown in the bottom.

C. APs (upper traces) and photo-activated currents (lowers traces) were evoked by delivering brief (1 ms) pulses of blue light (blue traces). FS IN was holding at -70 mV in current-clamp and voltage clamped at -70 mV.

D. Reconstruction of the same recorded PV$^+$ fast-spiking IN in A_1.

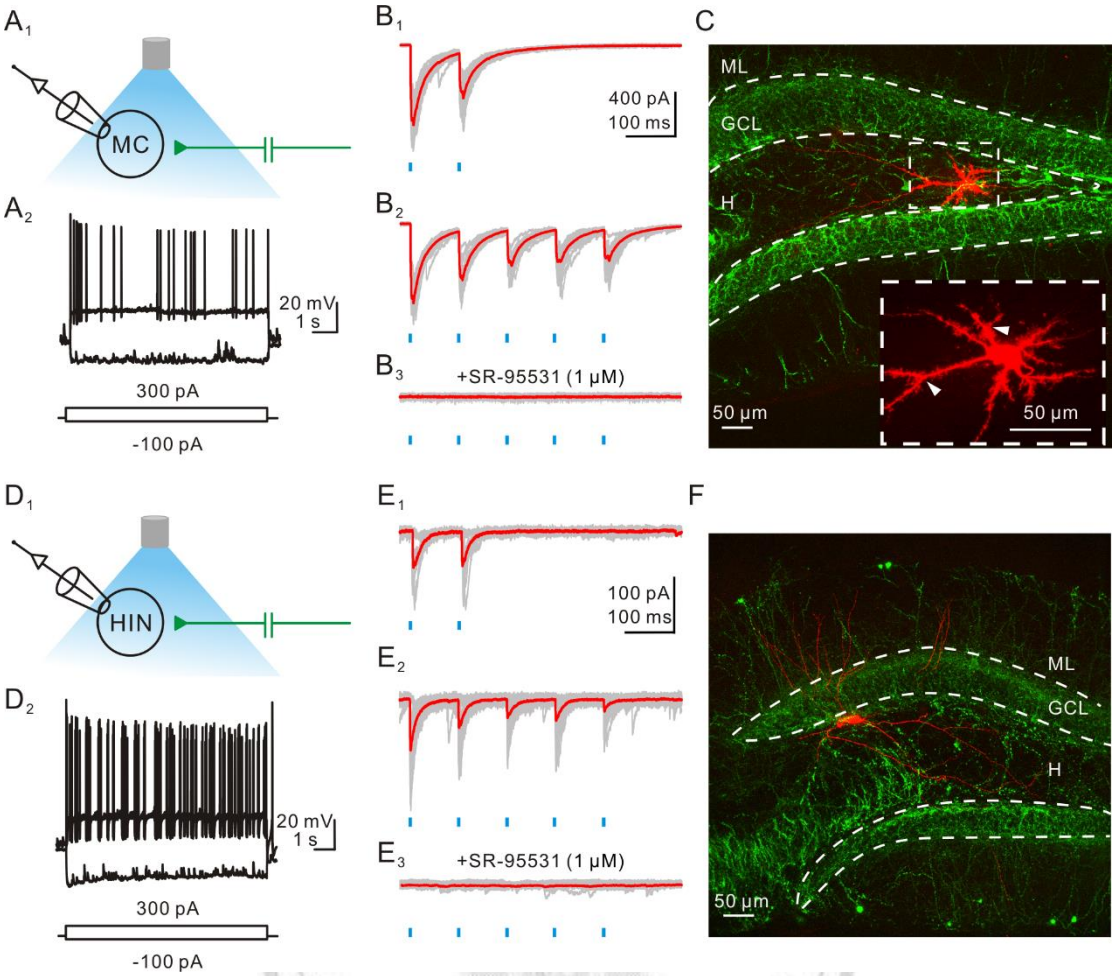

Figure 3. Functional connections of PV$^+$ IN-MC and PV$^+$ IN-HIN synapses

A_1, D_1. Experimental scheme showing optical activation of PV$^+$ axons with a patch-clamp recording from an MC (A_1) and an HIN (D_1).

A_2, D_2. Firing pattern and hyperpolarized membrane responses induced in the MC and HIN by the protocol shown in the bottom.

B_1, E_1. Photo-stimulation evoked IPSCs (averaged traces, red) recorded in the MC and HIN (blue traces, interpulse interval: 100 ms) in the presence of kynurenic acid (2 mM). Gray traces were individual IPSCs (30 sweeps).

B_2, E_2. Similar to B1 and E1, 10 Hz photo-stimulation (blue traces) evoked IPSCs, displaying multiple-pulse depression.

B_3, E_3. IPSCs were blocked by SR 95531 (1 μM).

C. Merged fluorescence image of ChR2-eYFP (green) expression and biocytin (red) staining of a representative MC in the hilus. The boxed area is shown at higher magnification (60x) in the inset. Arrowhead indicated complex spines known as thorny excrescences.

F. Merged fluorescence image of ChR2-eYFP (green) expression and biocytin (red) staining of a representative HIN at the border between the GCL and hilus. Note that complex spines were not detected in the HIN.

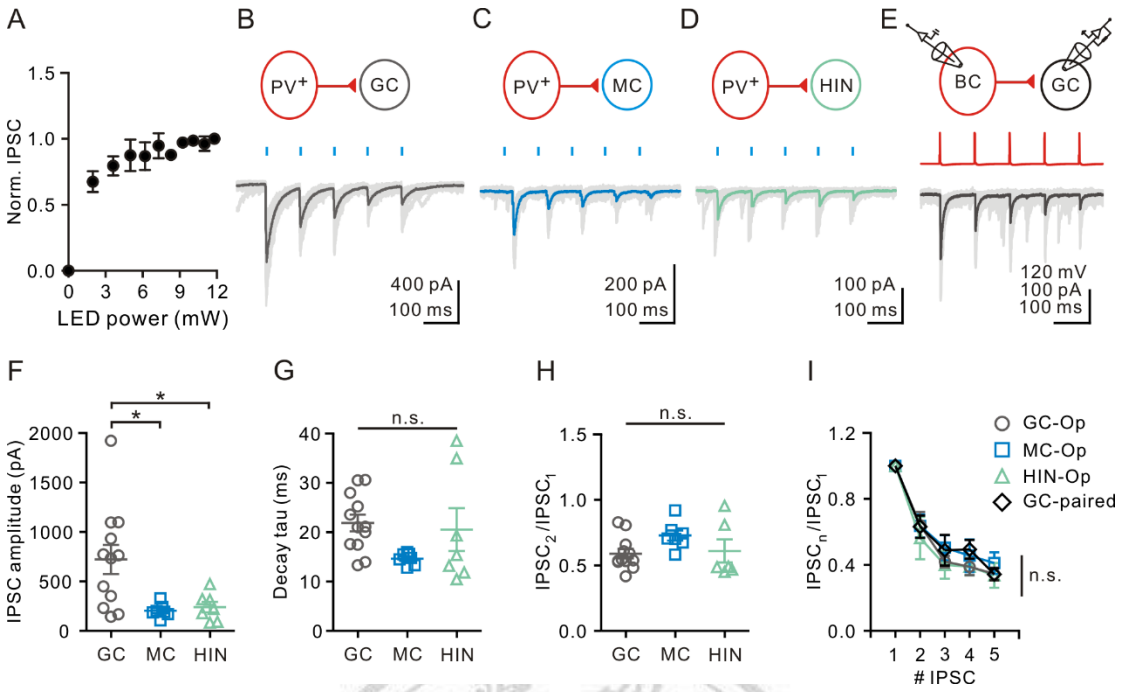

Figure 4. The functional properties of GCs, MCs and HINs

A. The plot showing normalized IPSC amplitude versus LED power intensity.

B-D. Top: schematic diagram illustrates PV^+ IN-GC, PV^+ IN-MC and PV^+ IN-HIN synapses. Bottom: averaged IPSCs in GCs (dark gray trace), MCs (dark blue trace), HINs (green trace) evoked by 10 Hz photo-stimulation (blue traces). Light gray traces were individual IPSCs (30 sweeps).

E. Top: schematic of paired recording from a FS IN to GC pair. Middle: five APs were evoked in the FS IN by injection of brief current pulses (1 ms, 10 Hz). Bottom: averaged IPSCs in GCs (red trace) were evoked by presynaptic FS IN. Presynaptic FS INs were current clamped at -70 mV, whereas postsynaptic GCs were voltage clamped at -80 mV.

F. Summary of peak amplitude of IPSCs in GCs, MCs and HINs (*$p < 0.05$, Wilcoxon-signed rank test).

G. Summary of decay time constant of IPSCs in GCs, MCs and HINs ($p = 0.3679$, n.s., not significant, Kruskal-Wallis test).

H. Summary of paired-pulse ratio of IPSCs in GCs, MCs and HINs ($p = 0.3679$, n.s.,

Kruskal-Wallis test).

I. Summary of multiple-pulse ratio of PV^+ IN-GC, PV^+ IN-MC, PV^+ IN-HIN, and BC-GC synapses ($p = 0.6697$, n.s., Kruskal-Wallis test).

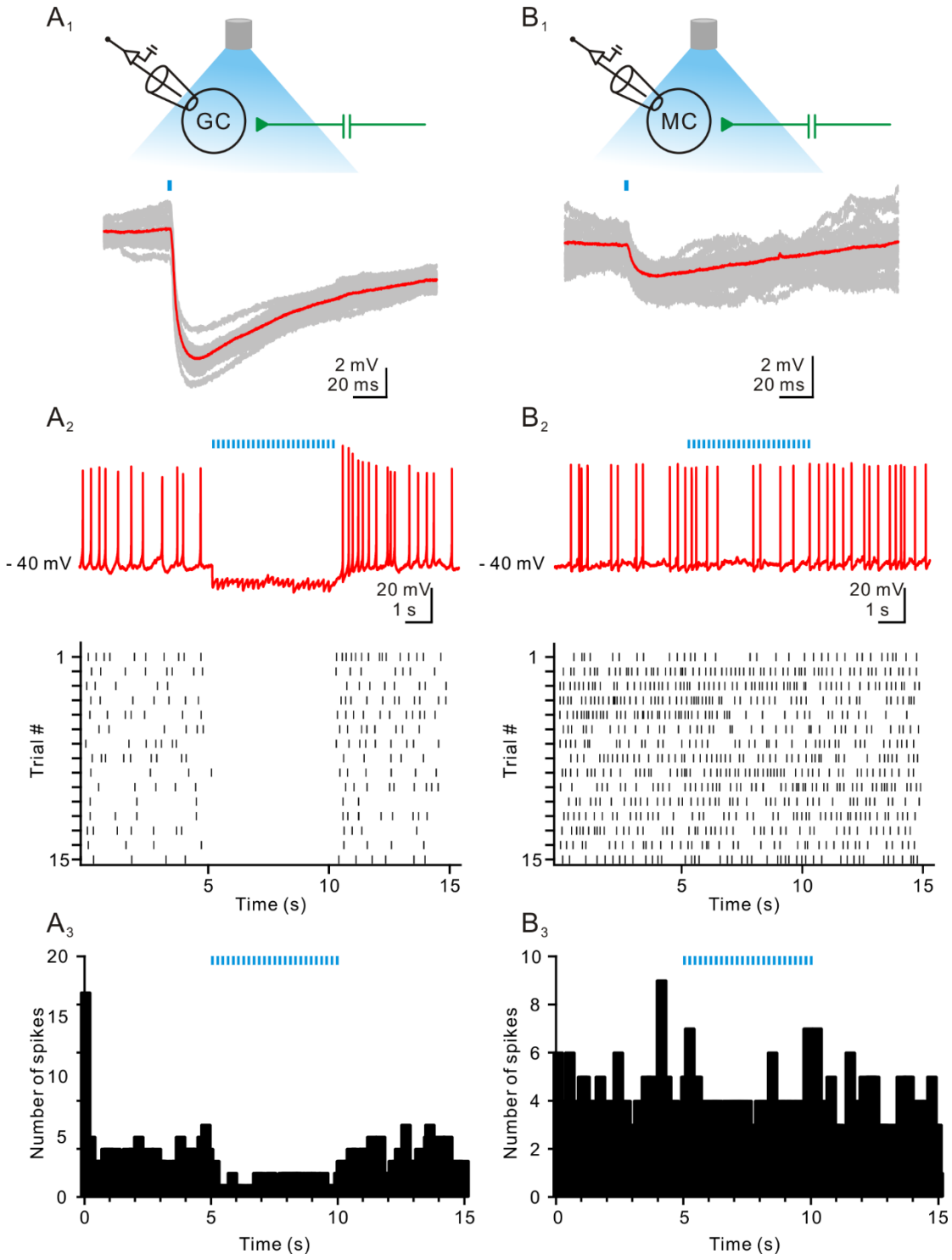

Figure 5. PV$^+$ INs provide stronger inhibition on GCs than MCs

A_1, B_1. Top: experimental scheme showing optical activation of PV$^+$ axons with patch-clamp recordings of a GC and MC. Bottom: light-evoked IPSPs (average traces, red) recorded in a single GC and MC held at -40 mV in current-clamp. Light gray traces were individual IPSPs (30 sweeps).

A_2, B_2. Top: blue light stimulation (5 Hz) evoked marked hyperpolarized potentials in GCs but not in MCs. Cells were held at -40 mV in current-clamp in the presence of 10 μM carbachol. Bottom: raster plot of spikes before, during and after photo-stimulation from GCs, and MCs.

A_3, B_3. Spike histogram of a single GC and MC as in A2, B2. Note that less spikes in the GC during photo-stimulation (blue traces).

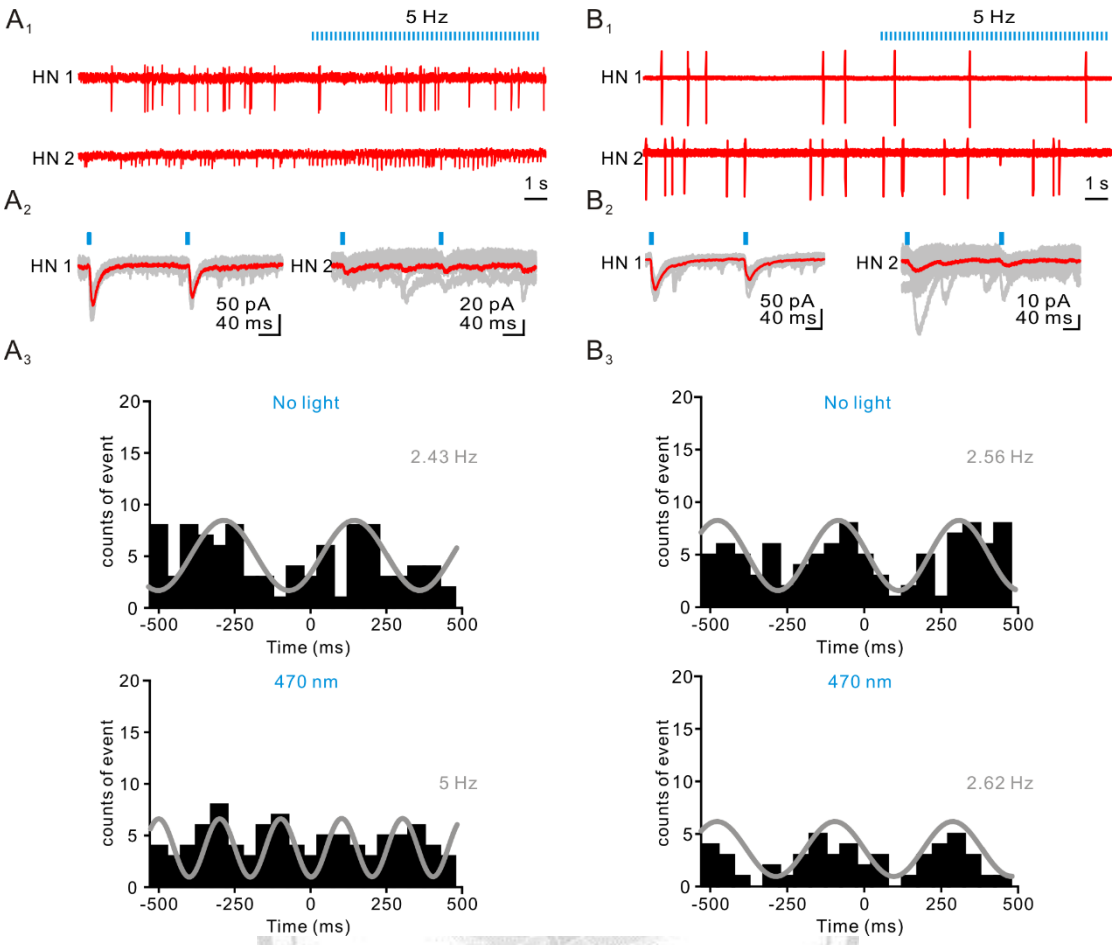

Figure 6. PV$^+$ IN-mediated GABA release may mediate synchronization between two HNs

A_1, B_1. Simultaneous cell-attached recording (red trace) from two HNs by delivering 5 Hz blue light stimulation (blue traces).

A_2, B_2. Whole-cell recording configuration showed that PV$^+$ INs innervated HN1 and HN2 (red traces) by delivering 5 Hz blue light stimulation (blue traces). Light gray traces represented individual IPSCs (30 sweeps).

A_3, B_3. Cross-correlation analysis of two HNs as in A_1, B_1. A_3 showed that synchronization between two HNs during photo-stimulation. B_3 showed that two HNs did not show the synchronization during 5 Hz photo-stimulation. The superimposed green traces showed sine waves of 5 Hz (A_3) and 2.62 Hz (B_3).

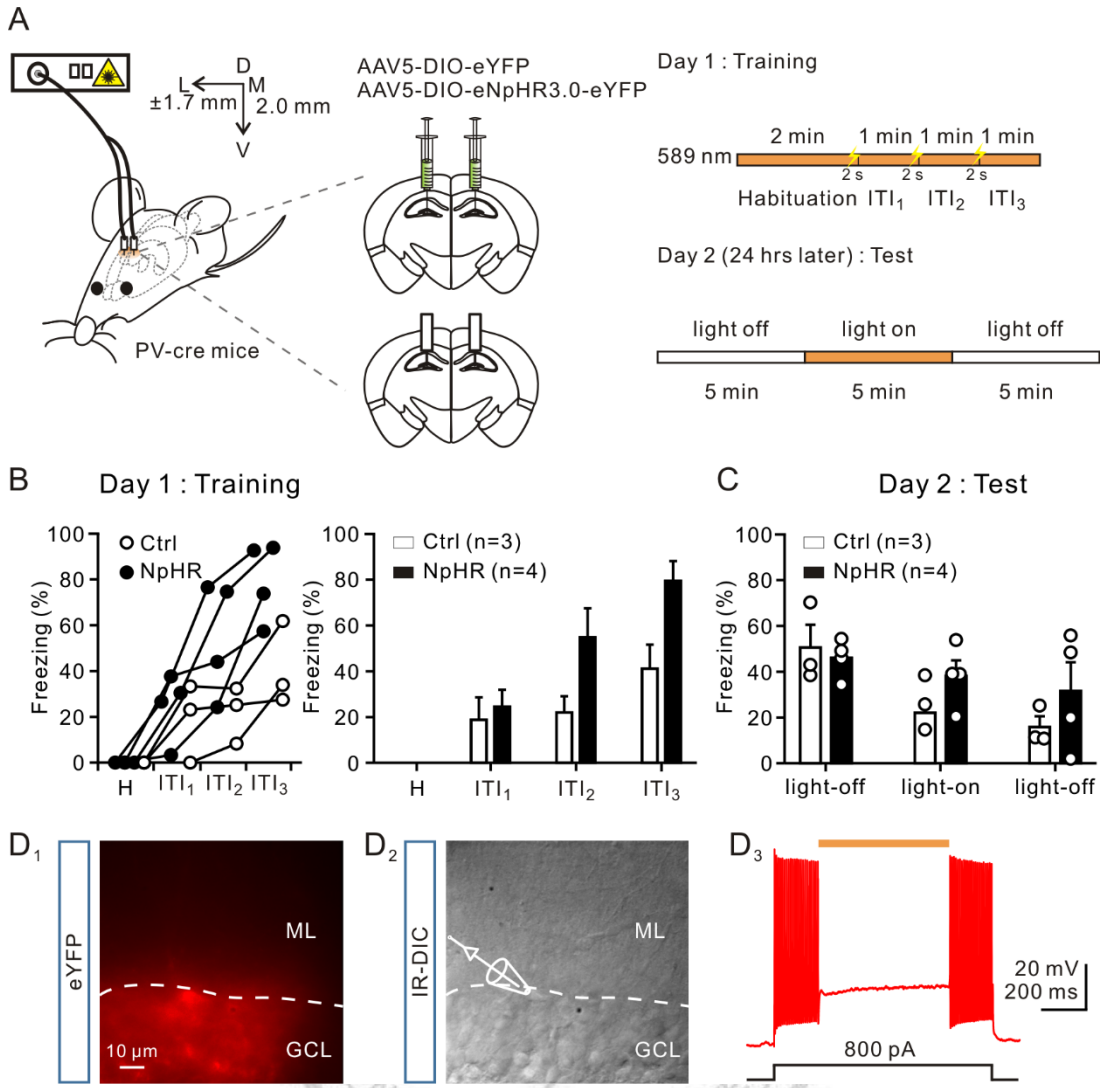

Figure 7. Silencing PV$^+$ INs in the DG improves fear learning

A. Left: schematic diagram of AAV5-DIO-eYFP or AAV5-DIO-eNpHR-eYFP injection and optical fiber implantation into both dorsal hippocampi of PV-cre mice for the contextual fear test. Right: the protocol of contextual fear test. On Day 1, mice were placed into the chamber box to habituate for 2 min. After 2-min habituation, mice received 3 trials (ITI, inter-trial interval: 1 min) of foot shock (0.6 mA, 2 s) in the following 3 min. Twenty-four hours later, mice were first placed into the chamber for 5 min without foot shock and light to assess the contextual fear, then followed by the light on for 5 min and finally light off for 5 min. The fiber-optic cannula were connected to optical fiber cables. The yellow light (10 mW) was delivered through the optical fibers

from the 589 nm DPSS laser as indicated.

B. Left: the percentage of freezing time was calculated for each mouse during the H (habituation), ITI_1, ITI_2, ITI_3 periods of training. The open circle represents the control group (eYFP), whereas the filled circle represents the NpHR group (eNpHR3.0-eYFP). Right: the percentage of freezing behavior of control and NpHR groups. Data represent mean ± SEM. Note that mice with silencing of PV^+ INs showed better learning behavior during training.

C. The percentage of freezing time during the test period on Day 2. Note that freezing level was not affected by optogenetic inhibition of PV^+ INs.

D_1. Fluorescence image of an eNpHR-$eYFP^+$ neuron, suggesting PV^+ IN. The borders of GCL are outlined. GCL, granule cell layer; ML, molecular layer.

D_2. IR-DIC image of the recorded PV^+ IN shown in D_1.

D_3. High-frequency APs were elicited in the same eNpHR-$eYFP^+$ neuron and suppressed during yellow light illumination. The time course of depolarizing current step was shown in the bottom.

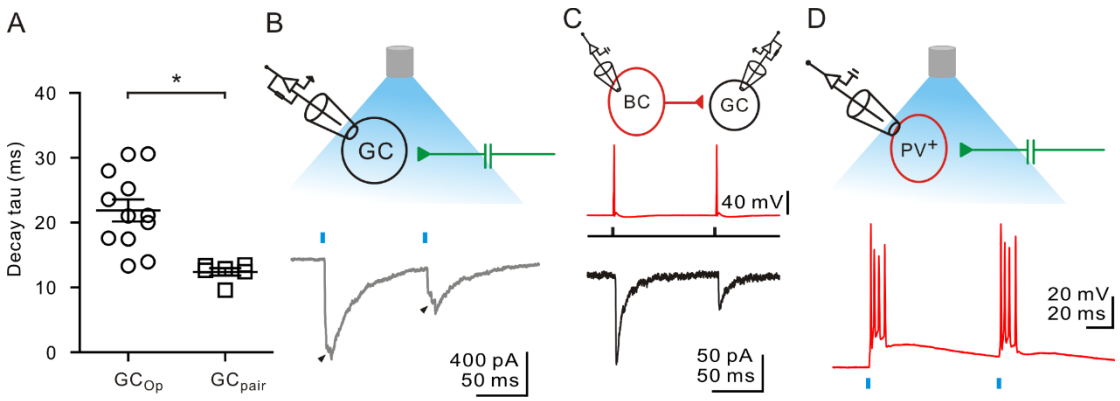

Figure 8. Differences in IPSCs evoked by optical stimulation and paired recording

A. Summary of decay time constant of IPSCs in GCs evoked by optical stimulation (GC_{Op}, n = 12) and direct AP generation in presynaptic FS INs (GC_{pair}; n = 6) (*$p < 0.05$, Wilcoxon-signed rank test).

B. Top: schematic of optical activation of PV^+ axons with whole-cell patch-clamp recordings of a GC. Bottom: photo-stimulation (blue, interpulse interval: 100 ms) evoked IPSCs (a single sweep, gray) recorded in the GC in the presence of kynurenic acid (2 mM). Arrowheads indicate asynchronous compound IPSCs.

C. Top: two consecutive APs (red trace) were evoked in the FS IN by injection of brief current pulses (black trace, 3 nA/ 1 ms; interpulse interval: 100 ms). Bottom: a single IPSC in GCs (black) were evoked by AP induction in a presynaptic FS IN. Presynaptic FS INs were current clamped at -70 mV, whereas postsynaptic GCs were voltage clamped at -80 mV. Note the faster decay of the unitary IPSC evoked by a single presynaptic FS IN.

D. Top: schematic of optical activation of PV^+ axons with whole-cell patch-clamp recording of a PV^+ IN. Bottom: APs (upper trace) were evoked by delivering brief light pulses (blue, 1 ms). The FS IN was held at -70 mV in current-clamp.

References

Acsády L, Kamondi A, Sik A, Freund T, Buzsaki G (1998) GABAergic cells are the major postsynaptic targets of mossy fibers in the rat hippocampus. J Neurosci 18:3386–3403.

Acsády L, Katona I, Martínez-Guijarro FJ, Buzsáki G, Freund TF (2000) Unusual target selectivity of perisomatic inhibitory cells in the hilar region of the rat hippocampus. J Neurosci 20:6907–6919.

Amaral DG (1978) A Golgi study of cell types in the hilar region of the hippocampus in the rat. J. Comp. Neurol 15:851–914.

Amaral DG, Ishizuka N, Claiborne B (1990) Neurons, numbers and the hippocampal network. Prog Brain Res 83:1–11.

Bartos M, Vida I, Jonas P (2007) Synaptic mechanisms of synchronized gamma oscillations in inhibitory interneuron networks. Nat Rev Neurosci 8:45–56.

Buzsáki G, Eidelberg E (1981) Commissural projection to the dentate gyrus of the rat: evidence for feed-forward inhibition. Brain Res 230:346–350.

Buzsáki G, Draguhn A (2004) Neuronal oscillations in cortical networks. Science 304:1926–1929.

Buzsáki G, Wang X (2012) Mechanisms of gamma oscillations. Annu Rev Neurosci 35:203–225.

Chiu CQ, Lur G, Morse TM, Carnevale NT, Ellis-Davies GC, Higley MJ (2013) Compartmentalization of GABAergic inhibition by dendritic spines. Science 340:759–762.

Cobb SR, Buhl EH, Halasy K, Paulsen O, Somogyi P (1995) Synchronization of neuronal activity in hippocampus by individual GABAergic interneurons. Nature 378:75–78.

Cruikshank SJ, Urabe H, Nurmikko AV, Connors BW (2010) Pathway-specific feedforward circuits between thalamus and neocortex revealed by selective optical stimulation of axons. Neuron 65:230–245.

Douglas RM, McNaughton BL, Goddard GV (1983) Commissural inhibition and facilitation of granule cell discharge in fascia dentata. J Comp Neurol 219:285–294.

Freund TF, Buzsáki G (1996) Interneurons of the hippocampus. Hippocampus 6:347–470.

Geiger JRP, Jonas P (2000) Dynamic control of presynaptic Ca^{2+} inflow by fast-inactivating K^+ channels in hippocampal mossy fiber boutons. Neuron 28:927–939.

Goodman JH, Sloviter RS (1992) Evidence for commissurally projecting parvalbumin-immunoreactive basket cells in the dentate gyrus of the rat. Hippocampus 2:13–21.

Han ZS, Buhl EH, Lörinczi Z, Somogyi P (1993) A high degree of spatial selectivity in the axonal and dendritic domains of physiologically identified local-circuit neurons in the dentate gyrus of the rat hippocampus. Eur J Neurosci 5:395–410.

Henze DA, Buzsáki G (2007) Hilar mossy cells: functional identification and activity in vivo. Prog BrainRes 163:199–216.

Hernández-Rabaza V, Hontecillas-Prieto L, Velázquez-Sánchez C, Ferragud A, Pérez-Villaba A, Arcusa A, Barcia JA, Trejo JL, Canales, JJ (2008) The hippocampal dentate gyrus is essential for generating contextual memories of fear and drug-induced reward. Neurobiology of Learning & Memory 90:553–559.

Hosp JA, Strüber M, Yanagawa Y, Obata K, Vida I, Jonas P, Bartos M (2014) Morpho-physiological criteria divide dentate gyrus interneurons into classes. Hippocampus 24:189–203.

Hurst JL, West RS (2010) Taming anxiety in laboratory mice. Nat Methods 7:825–826.

Ishizuka S, Kosaka T (1998) Physiological properties of mouse hippocampal mossy

cells. Neuroreport 9:193–199.

Ishizuka N (2001) Laminar organization of the pyramidal cell layer of the subiculum in the rat. J Comp Neurol 435:89–110.

Jackman SL, Beneduce BM, Drew IR, Regehr WG (2014) Achieving high-frequency optical control of synaptic transmission. J Neurosci 34:7704–7714.

Jinde S, Zsiros V, Jiang Z, Nakao K, Pickel J, Kohno K, Belforte JE, Nakazawa K (2012) Hilar mossy cell degeneration causes transient dentate granule cell hyperexcitability and impaired pattern separation. Neuron 76:1189–1200.

Josselyn SA (2010) Continuing the search for the engram: examining the mechanism of fear memories. J Psychiatry Neurosci 35:221–228.

Klausberger T, Somogyi P (2008) Neuronal diversity and temporal dynamics: the unity of hippocampal circuit operations. Science 321:53–57.

Kraushaar U, Jonas P (2000) Efficacy and stability of quantal GABA release at a hippocampal interneuron-principal neuron synapse. J Neurosci 20:5594–5607.

Leão RN, Mikulovic S, Leão KE, Munguba H, Gezelius H, Enjin A, Patra K, Eriksson Loew LM, Tort AB, Kullander K (2012) OLM interneurons differentially modulate CA3 and entorhinal inputs to hippocampal CA1 neurons. Nat Neurosci 15:1524–1530.

Larimer P, Strowbridge BW (2008) Nonrandom local circuits in the dentate gyrus. J Neurosci 28:12212–12223.

Lisman JE (1999) Relating hippocampal circuitry to function: recall of memory sequences by reciprocal dentate-CA3 interactions. Neuron 22:233–242.

Letzkus JJ, Wolff SBE, Meyer EMM, Tovote P, Courtin J, Herry C, Lüthi A (2011) A disinhibitory microcircuit for associative fear learning in the auditory cortex. Nature 480:331–335.

Leutgeb JK, Leutgeb S, Moser MB, Moser EI (2007) Pattern separation in the dentate gyrus and CA3 of the hippocampus. Science 315:961–966.

Lien CC, Mu Y, Vargas-Caballero M, Poo MM (2006) Visual stimuli induced LTD of GABAergic synapses mediated by presynaptic NMDA receptors. Nat Neurosci 9:372–380.

Liu X, Ramirez S, Pang PT, Puryear CB, Govindarajan A, Deisseroth K, Tonegawa S (2012) Optogenetic stimulation of a hippocampal engram activates fear memory recall Nature 484:381–385.

Liu YC, Cheng JK, Lien CC (2014) Rapid dynamic changes of dendritic inhibition in the dentate gyrus by presynaptic activity patterns. J Neurosci 34:1344–1357.

McHugh TJ, Jones MW, Quinn JJ, Balthasar N, Coppari R, Elmquist JK, Lowell BB, Fanselow MS, Wilson MA, Tonegawa S (2007) Dentate gyrus NMDA receptors mediate rapid pattern separation in the hippocampal network. Science 317: 94–99.

Miles R, Tóth K, Gulyás AI, Hájos N, Freund TF (1996) Differences between somatic and dendritic inhibition in the hippocampus. Neuron 16:815–823.

Moser EI, Kropff E, Moser MB (2008) Place cells, grid cells, and the brain's spatial representation system. Annu Rev Neurosci 31:69–89.

Murakawa R, Kosaka T (2001) Structural features of mossy cells in the hamster dentate gyrus, with special reference to somatic thorny excrescences. J Comp Neurol 429:113–126.

Myers CE, Scharfman HE (2009). A role for hilar cells in pattern separation in the dentate gyrus : a computational approach. Hippocampus 19:321–337.

Naber PA, Witter MP (1998) Subicular efferents are organized mostly as parallel projections: a double-labeling, retrograde-tracing study in the rat. J Comp Neurol 393:284–297.

Nakashiba T, Young JZ, McHugh TJ, Buhl DL, Tonegawa S (2008) Transgenic inhibition of synaptic transmission reveals role of CA3 output in hippocampal learning. Science 319:1260–1264.

Nevet A, Morris G, Saban G, Arkadir D, Bergman H (2007) Lack of spike-count and spike-time correlations in the substantia nigra reticulata despite overlap of neural responses. J Neurophysiol 98:2232–2243.

O'Keefe J, Dostrovsky J (1971) The hippocampus as a spatial map. Preliminary evidence from unit activity in the freely-moving rat. Brain Res 34:171–175.

Olsen SR, Bortone DS, Adesnik H, ScanzianiM (2012) Gain control by layer six in cortical circuits of vision. Nature 483:47–52.

Perkel DH, Gerstein GL, Moore GP (1967) Neuronal spike trains and stochastic point processes. II. Simultaneous spike trains. Biophys J 7:419–440.

Pouille F, Scanziani M (2001) Enforcement of temporal fidelity in pyramidal cells by somatic feed-forward inhibition. Science 293:1159–1163.

Rollenhagen A, Sätzler K, Rodríguez EP, Jonas P, Frotscher M, Lübke JHR (2007) Structural determinants of transmission at large hippocampal mossy fiber synapses. J Neurosci 39:10434–10444.

Santhakumar V, Bender R, Frotscher M, Ross ST, Hollrigel GS, Toth Z, Soltesz I (2000) Granule cell hyperexcitability in the early post-traumatic rat dentate gyrus: The "irritable mossy cell" hypothesis. J Physiol 524:117–134.

Scharfman HE (1995) Electrophysiological evidence that dentate hilar mossy cells are excitatory and innervate both granule cells and interneurons. J Neurophysiol 74:179–194.

Scharfman HE, Myers CE (2013) Hilar mossy cells of the dentate gyrus: a historical perspective. Frontiers Neural Circuits. Special issue on the Dentate Gyrus.

Schaffer K (1892) Beitrag zur histologie der Amnionshornformation. Arch Mikrosk Anat 39:611–632.

Somogyi P, Klausberger T (2005) Defined types of cortical interneurons structure space and spike timing in the hippocampus. J Physiol 562:9–26.

Sparta DR, Hovelsø N, Mason AO, Kantak PA, Ung RL, Decot HK, Stuber GD (2014) Activation of prefrontal cortical parvalbumin interneurons facilitates extinction of reward seeking behavior. J Neurosci 34:3699–3705.

Squire LR (1992) Memory and the hippocampus: a synthesis from findings with rats, monkeys, and humans. Psych Rev 99:195–231.

Szirmai I, Buzsáki G, Kamondi A (2012) 120 years of hippocampal schaffer collaterals. Hippocampus 22:1508–1516.

Varga C, Golshani P, Soltesz I (2012) Frequency-invariant temporal ordering of interneuronal discharges during hippocampal oscillations in awake mice. Proc Natl Acad Sci 109:E2726–E2734.

Wolff SB, Gründemann J, Tovote P, Krabbe S, Jacobson GA, Müller C, Herry C, Ehrlich I, Friedrich RW, Letzkus JJ, Lüthi A (2014) Amygdala interneuron subtypes control fear learning through disinhibition. Nature 509:453–458.

Zhang YP, Oertner TG (2007) Optical induction of synaptic plasticity using a light-sensitive channel. Nat Methods 4:139–141.